The Astrophysical Journal, 838:163 (15pp), 2017 April 1 https://doi.org/10.3847/1538-4357/aa6540

On the Origin of the Fundamental Plane and Faber–Jackson Relations: Implications for the Star Formation Problem

Mauro D'Onofrio[1], Stefano Cariddi[1], Cesare Chiosi[1], Emanuela Chiosi[1], and Paola Marziani[2]
[1] Department of Physics and Astronomy, University of Padova, Vicolo Osservatorio 3, I-35122 Padova, Italy; mauro.donofrio@unipd.it
[2] INAF—Padova Observatory, Vicolo Osservatorio 5, I-35122 Padova, Italy
Received 2016 December 9; revised 2017 February 4; accepted 2017 March 4; published 2017 April 5

Abstract

We provide an explanation of the properties of the fundamental plane (FP) relation and its observed projections for a sample of nearby early-type galaxies (ETGs) in terms of a fine-tuning between the time-averaged star formation rate $\langle\Psi\rangle$ and their structural and dynamical characteristics. Their total V luminosity is linked with $\langle\Psi\rangle$ and the central velocity dispersion σ through the relation $\log(L) = 0.48(\pm0.06)\log(\langle\Psi\rangle) + 1.00\,(\pm0.13)\log(\sigma) + 7.81(\pm0.26)$, with an rms $= 0.215$ ($R = 0.64$ and $P < 1.2 \times 10^{-16}$). This fine-tuning permits us to obtain the FP in terms of two distinct "virtual planes" in the $\log(R_e)-\log(\langle I_e\rangle)-\log(\sigma)$ space. The first one (the virial plane; VP) represents the total galaxy mass derived from the scalar virial theorem and the mass-to-light ratio M/L, while the second plane comes from the relation $L = L_0'\sigma^{-2}$, where L_0' is a parameter connected with $\langle\Psi\rangle$. This is a mathematically convenient way for expressing the independence of the galaxy light from the virial equilibrium. Each galaxy in the $\log(R_e)-\log(\langle I_e\rangle)-\log(\sigma)$ space is identified by the intersection of these two planes. A posteriori, we show that the properties of the FP (tilt and scatter) and the zone of exclusion visible in the FP projections are consequences of this fine-tuning. The link between the FP properties and the SFR of galaxies provides a new view of the star formation phenomenon. The star formation history of an unperturbed galaxy seems to be driven by the initial conditions in the protogalaxies and is regulated across cosmic epochs by the variation of the main galaxy parameters (mass, luminosity, structural shape, and velocity dispersion).

Key words: galaxies: evolution – galaxies: formation – galaxies: fundamental parameters – galaxies: star formation – galaxies: structure

1. Introduction

The origin of the fundamental plane (FP), i.e., the relation

$$a\log(R_e) + b\log(\langle I_e\rangle) + c\log(\sigma) + d = 0, \qquad (1)$$

between the effective surface brightness, the effective radius, and the central velocity dispersion of early-type galaxies (ETGs), is still unclear since the epoch of its discovery (Djorgovski & Davis 1987; Dressler et al. 1987). The problem is that the FP coefficients deviate from the virial expectation for homologous galaxies ($a \sim 1.2$ instead of 2 and $b \sim -0.7$ instead of -1) and the scatter around the plane is very small along the whole FP extension. The observed coefficients are found to depend on the filter band adopted (see, e.g., Scodeggio et al. 1998; Hyde & Bernardi 2009), on the fitting procedure (see e.g., Sheth & Bernardi 2012), and on the magnitude limit of the selected galaxy sample (see e.g., D'Onofrio et al. 2008), but in all cases they are significantly different from the virial expectation.

The first interpretation of the tilt was related to the behavior of the stellar populations of galaxies through their stellar mass-to-light ratios, which were seen to vary with luminosity ($M/L \sim M^{\alpha}$, with $\alpha \sim 0.25$ Faber et al. 1987). Subsequent, independent measurements found similar values of α (see e.g., Pahre et al. 1998; Borriello et al. 2001; Gerhard et al. 2001; Treu et al. 2005).

An alternative explanation was that galaxies are progressively non-homologous systems along the FP (Capelato et al. 1995; Hjorth & Madsen 1995; Busarello et al. 1997; Graham & Colless 1997; Prugniel & Simien 1997; Pahre et al. 1998; Bertin et al. 2002; Trujillo et al. 2004; Nipoti et al. 2006; La Barbera et al. 2010). This scenario was supported by the observation that the light profiles and dynamics of ETGs deviate systematically from homology (Michard 1985; Schombert 1986; Capaccioli 1987; de Carvalho & da Costa 1988; Capaccioli 1989; Burkert 1993; Caon et al. 1993; Young & Currie 1994; Prugniel & Simien 1997). Ciotti et al. (1996), however, pointed out that a strong fine-tuning between stellar mass-to-light ratio (M^*/L) and structure (Sérsic index n) is required to explain, using just structural non-homology, both the tilt of the FP and the small scatter around it (the so-called $M^*/L - n$ conspiracy). Cappellari et al. (2006, 2012) also excluded an important contribution of non-homology to the tilt using integral models of the ETGs' mass distributions, based on 2D kinematic maps. Along the same line, the galaxy-mass distribution estimated from gravitational lensing by Bolton et al. (2008) did not seem to support an important role for non-homology.

Subsequently, the interpretations of the tilt proposed a number of possible mechanisms: metallicity effects (Gerhard et al. 2001), dark matter (DM) distribution and amount (Secco 2001; Secco & Bindoni 2009; Tortora et al. 2009), dissipation effects during galaxy collapse (see, e.g., Oñorbe et al. 2005; Dekel & Cox 2006; Robertson et al. 2006; Hopkins et al. 2008), variable initial mass function (IMF; Chiosi et al. 1998), star formation history (SFH), etc., but the contribution of DM and IMF was also excluded by Ciotti et al. (1996) on the basis of a required strong fine-tuning argument, and the observation that the observed SFH of galaxies is hardly reconciled with the widely accepted hierarchical paradigm of the ΛCDM cosmology.

More recently, D'Onofrio et al. (2013) proposed the existence of a fine-tuning mechanism capable of explaining

the properties of the FP based on the observed mutual correlation between galaxy mass, mass-to-light ratio, and Sérsic index. Increasing evidence suggests that the main driver of stellar population properties in ETGs is the velocity dispersion, with a second-order effect due to galaxy environment (see, e.g., La Barbera et al. 2014). The slope of the IMF, for example, has been found to correlate with σ (Cenarro et al. 2001; van Dokkum & Conroy 2010; La Barbera et al. 2013). At the same time, merging events, gas accretion, and feedback processes seem to have a significant role in the evolution of ETGs, in particular in the center of groups and clusters. The question therefore is, to what extent have all these processes affected the FP properties of the nearby ETGs we see today?

In addition to the tilt, the small observed scatter (∼20%–25%) around the FP is also unexplained. Forbes et al. (1998) and Terlevich & Forbes (2002) found a correlation between the residuals of the FP and the age of the galaxies (ETGs with higher/lower surface brightness have younger/older ages). Gargiulo (2009) claimed that the FP residuals anti-correlate with the mean stellar age, while a strong correlation exists with [α/Fe]. Graves et al. (2009) proposed that the stellar population variations contribute at most 50% of the total thickness and that correlated variations in the IMF or in the central DM fraction make up the rest. Magoulas et al. (2012) found that the residuals about the FP show significant trends with environment, morphology, and stellar population, with the strongest trend being with age. Unfortunately, even if the data are even better today, the systematic errors in age, [Z/H], and [α/Fe] are still large and not well understood, as different packages for stellar population synthesis provide very different results.

The above discussion clearly reveals that a general consensus about the origin of the FP and its properties is still lacking. We note that even the distribution of galaxies in the $\log(\langle I_e\rangle)-\log(R_e)$ plane, i.e., one of the projections of the FP, is poorly understood. Kormendy (1977) showed that ETGs do not follow the distribution expected for galaxies of the same total luminosity, but are tilted with respect to this line, while Bender et al. (1992) and Burstein et al. (1997) noted that in this plane galaxies seem to avoid a region of space: the so-called zone of exclusion (ZOE). They claimed that the slope of the ZOE and the progressive displacement of the Hubble types from this line are consistent with the hierarchical clustering scenario with a $n = 1.8$ power-law density fluctuation spectrum (plus dissipation).

The same considerations can be done for the Faber–Jackson (FJ) relation connecting galaxy luminosity with velocity dispersion ($L \propto \sigma^{\sim 4}$; Faber & Jackson 1976), whose slope (and zero-point) changed progressively (today the measured slope is ∼2.0). This relation is considered a projection of the FP and as such was also related to the virial theorem, but alternative explanations are possible.

In this paper we do not want to provide a new fitting technique for getting the FP coefficients; our aim is to propose a new possible interpretation for the origin of the FP and FJ relations that can explain their observational properties. The paper is organized as follows. In the first section we present the main equations and assumptions that define the FP problem. In Section 3 we describe our proposed solution, and in Section 4 we provide the observational evidence in favor of our hypothesis. In Section 5 we investigate the connection between the SFR and the galaxy dynamics. In Section 6 we discuss the origin of the FJ and PFJ relations, and in Section 7 we discuss the consequences of our solution for the problem of the star formation activity in galaxies across cosmic history. Finally, in Section 8 we draw our conclusions.

2. The FP Problem

We assume that ETGs are gravitationally bound stellar systems that satisfy the virial theorem equation,

$$\langle V^2\rangle = \frac{GM_{\rm tot}}{\langle R\rangle}, \tag{2}$$

where $M_{\rm tot}$ is the total galaxy mass, $\langle R\rangle$ is a suitable mean radius, and $\langle V^2\rangle$ is a mean kinetic energy per unit mass. By definition every kind of virialized system must belong to the virial plane (VP) in the space defined by the variables $M_{\rm tot}$, $\langle R\rangle$, and $\langle V^2\rangle$. Unfortunately, these are not observable quantities. Therefore, in the case of ETGs, the virial Equation (2) is usually written as follows:

$$M_{\rm tot} = \frac{K_V \sigma^2 R_e}{G}, \tag{3}$$

where R_e is the effective radius and $K_V = 1/(k_v k_r)$ takes into account projection effects, density distribution, and stellar orbit distribution. The term K_V parameterizes our ignorance about the orientation, 3D structure, and dynamics of ETGs. The formal expression of K_V (which is a dimensionless quantity) assumes $\langle V^2\rangle = k_v\sigma^2$ and $\langle R\rangle = k_r R_e$.

Introducing the mean effective surface brightness $\langle I\rangle_e = L/2\pi R_e^2$, one finds such an expression for the VP:

$$R_e = \frac{K_V}{2\pi G}\left(\frac{M_{\rm tot}}{L}\right)^{-1}\langle I_e\rangle^{-1}\,\sigma^2, \tag{4}$$

or, in logarithmic form:

$$\log(R_e) = 2\log(\sigma) - \log(\langle I_e\rangle) + \log(K_V) - \log\left(\frac{M_{\rm tot}}{L}\right) - \log(2\pi G). \tag{5}$$

This formulation of the virial theorem is directly comparable with the FP of Equation (1), rewritten with $\log(R_e)$ as an independent variable empirically derived from observations.

Note that for a given mass $M_{\rm tot}$ and zero-point there are infinite values of $\log(R_e)-\log(\langle I_e\rangle)-\log(\sigma)$ that satisfy Equation (5): all the points belonging to a plane obey such an equation. We can therefore define the VP as the locus of points of the $\log(R_e)-\log(\langle I_e\rangle)-\log(\sigma)$ space that reproduce a constant mass $M_{\rm tot}$ for an assigned zero-point.

The zero-point of Equation (5) is given by the quantity

$$\mathrm{ZP_{FP}} = \log(K_V) - \log\left(\frac{M_{\rm tot}}{L}\right) - \log(2\pi G), \tag{6}$$

so each galaxy has its own zero-point characterized by a peculiar M/L (DM and stellar content) and K_V (degree of non-homology). If ETGs were perfectly homologous systems (same K_V) with similar M/L, the $\mathrm{ZP_{FP}}$ would be a constant and all galaxies would be distributed along one VP. In other words, the virial theorem does not provide any constraints on the position of a galaxy in the $\log(R_e)-\log(\langle I_e\rangle)-\log(\sigma)$ space. Two galaxies with the same mass and zero-point, but with a different combination of M/L and K_V, may share the same VP. In

general, Equation (5) defines a family of planes filling the $\log(R_e)-\log(\langle I_e\rangle)-\log(\sigma)$ space for all galaxies.

In the $\log(R_e)-\log(\langle I_e\rangle)-\log(\sigma)$ space each VP is parallel to the others, so in principle one should observe a cloud and not a plane, unless a mechanism constrains all galaxies on the observed FP.

The connection between the FP and the VP clearly links the tilt of the plane to the properties of the stellar population, to the DM content, and the galaxy structure and dynamics. It is therefore not surprising that all the proposed solutions have tried to demonstrate the link between the zero-point and these galaxy properties. The existence of the FP, with its tilt and small scatter, requires a connection between K_V (structure) and M/L (DM and stellar populations). This is the so-called fine-tuning problem.

3. The New Proposed Solution

The new proposed solution comes from the observation that a galaxy of a given mass $M_{\rm tot}$ does not have a defined position in the $\log(R_e)-\log(\langle I_e\rangle)-\log(\sigma)$ space. Its virial equilibrium is guaranteed by all possible combinations of the variables that fit the virial equation. It would be nice to have at least another constraint to better define the location of a galaxy in the $\log(R_e)-\log(\langle I_e\rangle)-\log(\sigma)$ space.

In order to find such a constraint we consider that a galaxy of a given mass $M_{\rm tot}$ has also a total luminosity $L_{\rm tot}$. The luminosity of a galaxy ultimately depends on the luminosities of its stars, which in turn depend on the star radius and the effective temperatures that each star reaches at its surface.

The common way of introducing the luminosity in the FP problem was through the mass-to-light ratio, but we note that luminosity is actually a quantity independent of the virial equilibrium, being only the product of the SF history of galaxies.

On the basis of such consideration we look for the various expressions that can give the total luminosity of galaxies. We know that the integrated bolometric luminosity L of a galaxy of age T_G can be expressed as

$$L(T_G)=\int_0^{\infty}\int_o^{T_G}\int_{M_L}^{M_U} S(M,\,t,\,Z(t))f_\lambda \times (M,\,\tau',\,Z(\tau'))dMdtd\lambda, \quad (7)$$

where $S(M,\,t,\,Z(t))$ is the stellar birthrate, $f_\lambda(M,\,\tau',\,Z(\tau'))$ is the monochromatic flux of a star of mass M, metallicity $Z(t)$, and age $\tau'=T_G-t$, and M_L and M_U are the minimum and maximum star masses that are formed. The stellar birthrate $S(M,\,t,\,Z(t))$ can be expressed as the total mass converted into stars per unit time (e.g., $M_\odot\,{\rm yr}^{-1}$) or the total number of stars formed per unit time at the time t with the chemical composition $Z(t)$. We adopt the first definition for the sake of consistency with the definition of other quantities in usage here that are related to the star formation. Separating the $S(M,\,t,\,Z(t))$ into the product of the SFR $\Psi(t,\,Z(t))$ and the IMF $\Phi(M,\,Z(t))$, and neglecting here the dependence on the metallicity (it can be easily introduced whenever necessary) the above integral becomes

$$L=\int_0^{\infty}\int_o^{T_G}\Psi(t)F_\lambda(\tau')dtd\lambda, \quad (8)$$

where

$$F_\lambda(\tau')=\int_{M_L}^{M_U}\Phi(M)f_\lambda(M,\,\tau')dM, \quad (9)$$

where $F_\lambda(M,\,\tau')$ is the integrated monochromatic luminosity at each epoch provided by a single stellar population of age τ' and $f_\lambda(M,\,\tau')$ is the monochromatic luminosity emitted by a star of mass M and age τ' or t in general. Finally, we define the luminosity per unit mass of a single stellar population (SSP) as

$$L_{\rm sp}(t)=\int_0^{\infty}F_\lambda(t)d\lambda, \quad (10)$$

and finally

$$L=\int_0^{T_G}\Psi(dt)L_{\rm sp}(t)dt. \quad (11)$$

We can rewrite Equation (11) for the total luminosity considering the average values of the involved variables as

$$L\;\sim\;\langle\Psi(t)\times L_{\rm sp}\rangle T_G\sim\langle\Psi\rangle\left\langle\frac{L}{M}\right\rangle T_G, \quad (12)$$

where $\langle\Psi(t)\rangle$ is the time average of the current SFR, and T_G is the age of the galaxy. In the above average, $\langle L/M\rangle$ indicates the mean stellar light-to-mass ratio representative of all the stellar contents. The total emitted light today is the result of the whole SFH, independent of the events that have contributed to the increase of the SFR or its quenching. We further note that within the time-averaged values of $\langle\Psi(t)\times L_{\rm sp}\rangle$ are encrypted the contributions of the IMF.

Recall that the luminosity of ETGs correlates with the velocity dispersion of their stars through the FJ relation (Faber & Jackson 1976). The best way to write this relation is

$$L=L_0\left(\frac{\sigma}{\sigma_0}\right)^{\beta}, \quad (13)$$

where σ_0 is a reference zero-point normalization in velocity dispersion, β is the exponent derived through the fit of the data (often written in log form) and L_0 is a reference luminosity for the galaxy with $\sigma=\sigma_0$. Measured values for β range from 2 to 5 depending on the width of the magnitude range and the luminosity of the sampled galaxies within the magnitude range (see, e.g., Nigoche-Netro et al. 2010).

The origin of this correlation is far from clear. Why in fact should L and σ be correlated variables? The SF is a local phenomenon originating from microphysical processes inside clouds of gas and dust, while the velocity dispersion of a galaxy is a direct consequence of the mass potential well. How do the two things communicate? A priori, there are no reasons at all for such a connection. Why should the galaxy dynamics be aware of the stars that have been produced across cosmic time? A posteriori, we understand the L–σ relation on the basis of the connection between mass and luminosity in each single star and on the basis of the virial theorem. We will explore this issue again later on.

In the following we will often prefer to write Equation (13) in the form $L=L_0\sigma^{\beta}$, i.e., dropping the term σ_0. In this way we can simplify the calculations as follows. For the moment we emphasize that in this form the parameter L_0 has units of $[{\rm gr\,s}^{-1}]$, i.e., they are consistent with a SFR if $\beta=2$.

A direct comparison of Equations (12) and (13) tells us that the parameter L_0 of the FJ relation is connected to the mean SFR. We can in fact write

$$L_0 = \langle \Psi(t) \times L_{\rm sp} \rangle T_G / \sigma^{\beta}. \quad (14)$$

In this parameter L_0 the complex relationship between the galaxy dynamics and the SFH is therefore encrypted.

Now, remembering that $L_{\rm tot} = 2\pi \langle I_e \rangle R_e^2$, and passing to the logarithms, Equation (13) (in its simplified form) can be rewritten as

$$\log(R_e) = (\beta/2)\log(\sigma) - (1/2)\log(\langle I_e \rangle) + (1/2)\log(L_0) - (1/2)\log(2\pi). \quad (15)$$

At this point we can consider Equations ((1) the FP), ((5): the VP) and ((15): the FJ) using σ as dependent variable:

$$\begin{aligned}
\log(\sigma) &= A\log(R_e) + B\log(\langle I_e \rangle) + C \\
\log(\sigma) &= \frac{1}{2}\log(R_e) + \frac{1}{2}\log(\langle I_e \rangle) + \frac{1}{2}\log(M/L) \\
&\quad - \frac{1}{2}\log(K_V) + \frac{1}{2}\log(2\pi G) \\
\log(\sigma) &= \frac{2}{\beta}\log(R_e) + \frac{1}{\beta}\log(\langle I_e \rangle) \\
&\quad - \frac{1}{\beta}\log(L_0) + \frac{1}{\beta}\log(2\pi), \quad (16)
\end{aligned}$$

where the coefficients A, B and C are related to those of Equation (1). Then we take the differences FP-VP and FP-FJ. These differences must be equal on the intersecting lines. It follows that:

$$\log(\langle I_e \rangle) = \frac{(2/\beta) - (1/2)}{(1/2) - (1/\beta)}\log(R_e) + \Pi, \quad (17)$$

where Π can be defined by:

$$\Pi = \frac{1}{2}\log(K') = \frac{\left[\frac{1}{2}\log(K_V) - \frac{1}{2}\log(M/L)\right]}{\left[\frac{1}{2} - \frac{1}{\beta}\right]} + \frac{\left[-\frac{1}{\beta}\log(L_0) - \frac{1}{2}\log(2\pi\ G) + \frac{1}{\beta}\log(2\pi)\right]}{\left[\frac{1}{2} - \frac{1}{\beta}\right]}. \quad (18)$$

This also defines the dimensional constant K'.

Now we ask if Equation (13) could represent the plane we are looking for in the $\log(R_e)-\log(\langle I_e \rangle)-\log(\sigma)$ space. First, we observe that in the FJ relation L_0 is nearly constant for almost all ETGs (in the mass range 10^9–$10^{12} M_\odot$) of different σ. The value of L_0 valid for all our ETGs is 1.6×10^{29} gr s^{-1}. So this relation is not the one we are looking for as a second virtual plane representing the total luminosity of a galaxy in the $\log(R_e)-\log(\langle I_e \rangle)-\log(\sigma)$ space. Furthermore, for $\beta = 2$, which is a good possible fit for the FJ relation (see Figure 1), in Equation (17) the slope of the I_e–R_e relation is undefined.

Looking at Figure 1 we note that there are alternative mathematically correct values of β that could give the total luminosity of a galaxy $L_{\rm tot}$. In other words we should find the correct value for β on the basis of the observed distribution of galaxies in the FP projections that provides the total luminosity of each single galaxy. We will see below that the best value for β is -2.

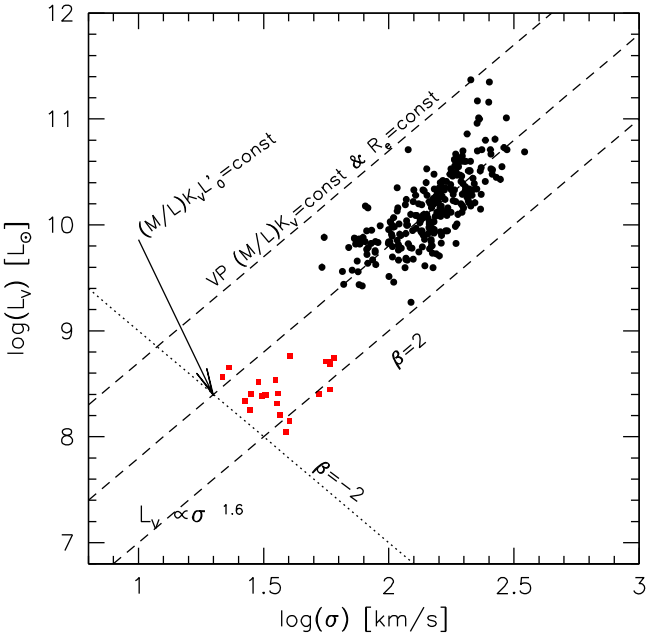

Figure 1. Distribution of ETGs in the L–σ plane. The dashed lines mark the position of the VPs ($\beta = 2$) for galaxies with different effective radii and zero-points. The dotted line marks one possible PFJ plane with $L_0' =$ constant, with a slope equal to -2 (see the text). The classical FJ relation seems to result from the intersection of the PFJ and the VP planes. The filled circles are normal ETGs. The red squares are dwarf galaxies of the WINGS database with masses around 10^8–$10^9 M_\odot$.

Figure 1 shows with dashed lines the slope of the $\beta = 2$ lines in the L–σ space. The dotted line marks the planes with $\beta = -2$. We will therefore write hereafter the relation of Equation (13) with $\beta = -2$ as $L = L_0' \sigma^{-2}$, again dropping the normalization constant but remembering that it is here. The values of L_0' are in this case the intercepts with the $\log(\sigma) = 0$ axis and have the same unit of L_0 (i.e., that of a characteristic luminosity). With this equation we can assign to L_0', which is very different from galaxy to galaxy, the primary role of capturing the SFH of each object, leaving to σ the secondary role of indicating how the velocity dispersion affects the SFR (note that σ could only change in the limited interval provided by the scatter of the FJ relation).

Since L_0' and L_0 correlated for $\beta = 2$, $L_0 = L_0' \sigma^{-4}$. It follows on the basis of Equation (12) that L_0' also is connected to the SFR:

$$L_0' = \langle \Psi(t)\, L_{\rm sp} \rangle T_G \sigma^2. \quad (19)$$

Now, substituting L_0' to L_0 in Equation (15) we obtain a plane in the $\log(R_e)-\log(\langle I_e \rangle)-\log(\sigma)$ space, which is tilted in the right direction with respect to the VP and has the notable property of having a significantly different zero-point for each galaxy.

This is the second virtual plane of the $\log(R_e) - \log(\langle I_e \rangle)-\log(\sigma)$ space that we are looking for. It represents the total luminosity of a galaxy with a zero-point different for each object, as is the case for the total mass in the VP (through (M/L) and K_V as zero-points).

We call this plane the "PFJ plane" (pseudo-FJ) to keep in mind its origin from the FJ relation, and we define it as follows: the PFJ plane is the locus of points defined by the values of $\log(R_e)-\log(\langle I_e \rangle)-\log(\sigma)$, which reproduce a constant luminosity $L_{\rm tot}$ for an assigned zero-point L_0'. This plane contains,

like the VP, only one galaxy, and all PFJ planes are parallel to each other in the $\log(R_e)-\log(\langle I_e\rangle)-\log(\sigma)$ space.

The different inclinations of the VP and PFJ planes suggest that they intersect somewhere in the $\log(R_e)-\log(\langle I_e\rangle)-\log(\sigma)$ space, forming a line in that space. Along this line resides only one object, the one with mass $M_{\rm tot}$, luminosity $L_{\rm tot}$, and zero-points $Z_{\rm FP}$ and $Z_{PFJ} = 1/2\log(L_0')$. In other words, along this line, the product $(M/L)K_V L_0'$ is constant.

It is clear that if the zero-points of the VP and PFJ planes vary in a coordinated way, the result will be the formation of several parallel lines in the $\log(R_e)-\log(\langle I_e\rangle)-\log(\sigma)$ space, each one containing one galaxy. The plane best fitting this distribution of parallel lines is the plane of real galaxies in the $\log(R_e)-\log(\langle I_e\rangle)-\log(\sigma)$ space, i.e., the FP. We therefore define the FP as follows: the FP is the plane in the $\log(R_e)-\log(\langle I_e\rangle)-\log(\sigma)$ space that best fits all the parallel lines formed by the intersections of the VP and PFJ planes. In this plane the quantity $(M/L)K_V L_0'$ is constant. In this framework, the existence of a FP for real galaxies implies that a close connection must exist between (M/L), K_V, and L_0' (or in other words between mass, luminosity, structure, and SFR).

A graphical sketch representing the mechanism at the origin of the FP is given in Figure 2. The upper panel of the figure shows two possible VPs for two galaxies (in black and gray) and one PFJ plane for one galaxy. The intersecting lines formed in the $\log(R_e)-\log(\langle I_e\rangle)-\log(\sigma)$ space by the VP and PFJ planes for galaxies of masses $M_{\rm tot}$ and luminosities $L_{\rm tot}$ mark the locus in which galaxies might reside.

Consequently, the FP plane is naturally tilted with respect to both the VP and PFJ planes. Its tilt is now connected to the global variation of the zero-points of the VP and PFJ planes ($Z_{\rm FP}$ and $Z_{\rm PFJ}$), and the small scatter observed around the plane originates from the fine-tuning effect linking M/L, K_V and L_0', i.e., linking the galaxy mass, structure and dynamics with the SFR of galaxies.

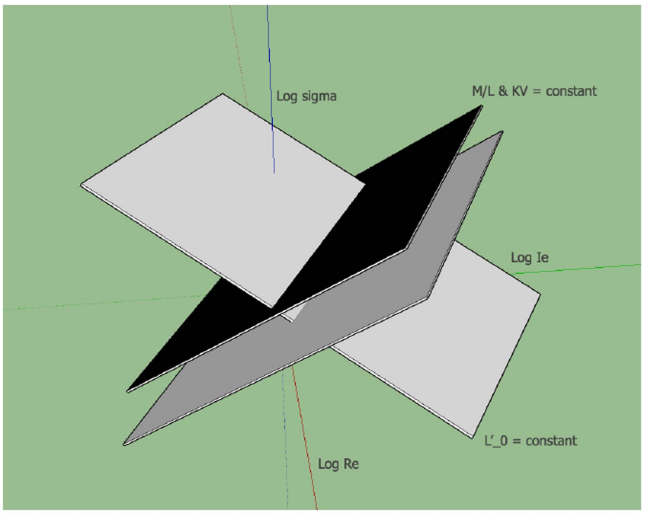

(a)

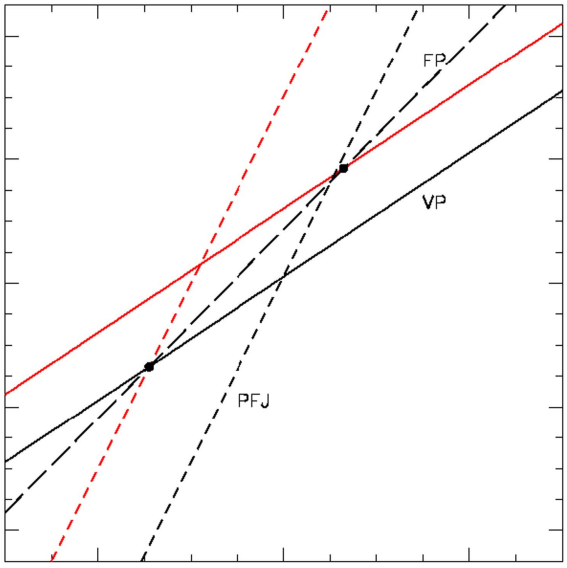

(b)

Figure 2. This figure aims to give a schematic idea of the mechanism originating the FP. Panel (a): general view of the $\log(R_e)-\log(\langle I_e\rangle)-\log(\sigma)$ space with two possible VPs and one PFJ plane. Panel (b): two possible VP and PFJ planes seen edge-on for two ETGs of masses M_1 and M_2 and luminosities L_1 and L_2, respectively, are shown with black (VP) and red lines (PFJ). The FP results in this case from the connection of the two intersections of the VP and PFJ planes. For many galaxies the FP is the plane best fitting all the intersecting lines.

4. The Observed Projections of the FP

Could we demonstrate observationally that the FP originates from the existence of the VP and PFJ planes?

Observations have shown that not only the FP of ETGs is tilted with respect to the VP and that the scatter around the plane is small ($\sim$20%), but also that the distribution of galaxies in the FP projections is far from random. The best known example is the $\langle\log(I)\rangle_e-\log(R_e)$ plane. Kormendy (1977) first noted a correlation between these variables with a slope different from that predicted on the basis of the total luminosity. Capaccioli et al. (1992), Bender et al. (1992), and Burstein et al. (1997) further noted that galaxies seem to avoid a region of this space: the ZOE.

We will see here that the projections of the FP, in particular the $\log(\langle I_e\rangle)-\log(R_e)$ plane, the $\log(\langle I_e\rangle)-\log(\sigma)$ plane, and the $\log(\sigma)-\log(R_e)$ plane can greatly help us to constrain the value of β.

For this task we use the data of the WIde-field Nearby Galaxy-cluster Survey (WINGS) database (Moretti et al. 2014). WINGS (Fasano et al. 2006) is a spectrophotometric survey of 76 X-ray selected galaxy clusters with redshifts $0.04 \lesssim z \lesssim 0.07$. The photometry in the B- and V-bands is from Varela et al. (2009), that for the J- and K-bands is from Valentinuzzi et al. (2009), and that for the U-band is from Omizzolo et al. (2009). Spectroscopic observations were performed by Cava et al. (2009) for a subsample of galaxies. Effective radii and surface brightness for normal ETGs and dwarfs were measured with GASPHOT by D'Onofrio et al. (2014) and galaxy morphologies with MORPHOT by Fasano et al. (2012). Central velocity dispersions were taken from the literature (Bernardi et al. 2003; Smith et al. 2004). For a subsample of the WINGS galaxies stellar masses and star formation rates were measured through the fitting of the SED by Fritz et al. (2007). He provided the SFR in four different cosmic epochs: (1) $2 \div 20$ Myr: stellar populations characterized by lines in emission and the strongest ultraviolet emission; (2) $20 \div 600$ Myr: in this age range the Balmer lines reach their maximum intensity in absorption, while the Cak line is almost nondetectable; (3) $0.6 \div 5.6$ Gyr: Balmer absorption lines are, as

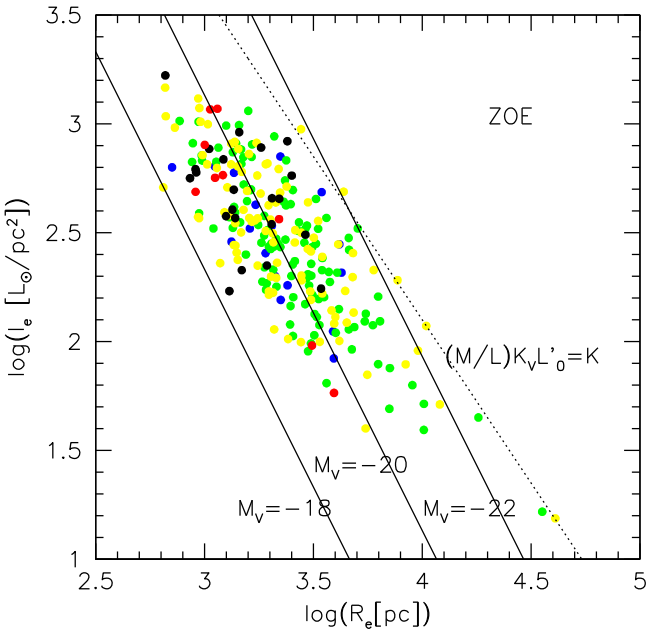

Figure 3. The $\log(\langle I_e\rangle)-\log(R_e)$ plane of the WINGS ETGs. Galaxies are plotted with different colors according to their measured stellar M^*/L (blue dots: $M^*/L = 1$; green: $M^*/L = 3$; yellow: $M^*/L = 5$; black: $M^*/L = 7$; red: $M^*/L > 8$). The solid lines give the locus of constant galaxy luminosity. The dotted lines mark the locus of constant M/L, K_V, and L_0', i.e., the projections of the intersecting lines originating the FP when $\beta = -2$.

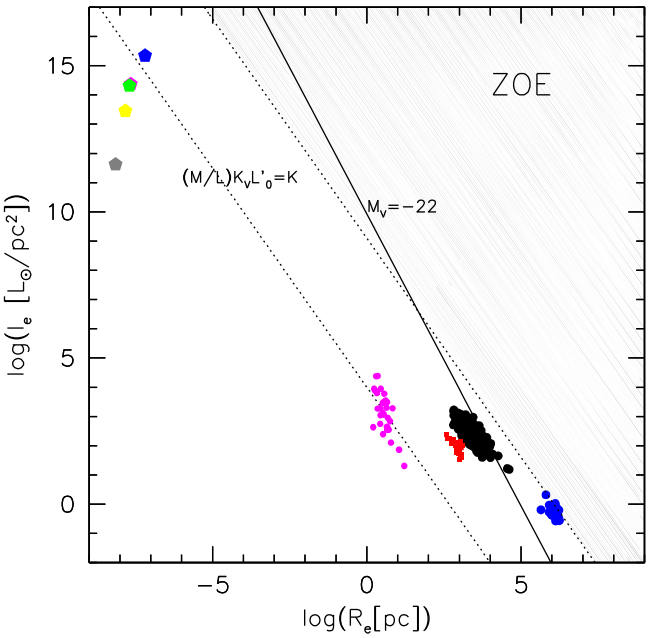

Figure 4. The $\log(\langle I_e\rangle)-\log(R_e)$ plane for objects of different masses that are known to be close to the virial equilibrium: main sequence stars (blue dot = α Cor B.; magenta = Sun; green = 70 Oph A, yellow = 61 Cyg A, gray = EZ Aqu.), globular clusters (GCs; magenta dots), dwarf galaxies (red dots), normal ETGs (black dots), and galaxy clusters (blue dots). The solid line gives the locus of constant absolute magnitude ($M_V = -22$), while the dotted lines are parallel to the ZOE and mark the positions of the different constant values of $(M/L)K_V L_0'$. The shaded area in gray is the ZOE.

the age increases, less intense in this age range, while the k line of calcium reaches its maximum intensity in absorption; (4) $5.6 \div 17.8$ Gyr: the main features reach an asymptotic value for these SSPs. With these data we define the time average $\langle\Psi\rangle$ as the sum of the four SFRs obtained for the different cosmic epochs.

In the previous section we obtained an equation for the distribution of galaxies with similar M/L, K_V, and L_0' in the $\log(\langle I_e\rangle)-\log(R_e)$ relation. The zero-point of Equation (17) varies as M/L, K_V, and L_0' vary in the FP space. Note that the slope of this relation depends only on the value of β, i.e., on the exponent of the PFJ plane.

The question therefore is, where are the projections of the intersecting lines located, i.e., the lines of constant M/L, K_V, and L_0' in these 2D planes?

Figure 3 shows the $\log(\langle I_e\rangle)-\log(R_e)$ plane where we have adopted the solution of Equation (18) with $\beta = -2$. Note how this value of β naturally reproduces the slope of the observed distribution of galaxies. It follows that the so-called ZOE is in this context a natural limit reached today by the values of M/L, K_V, and L_0' during the cosmic evolution. In the figure we plotted with different colors different ranges for the stellar M^*/L ratios available for the galaxies of the WINGS database in the V-band (Moretti et al. 2014). Note that there is not a clear trend of the galaxy distribution with the M^*/L ratios, even if the higher mass-to-light ratios seem more frequently distributed far from the ZOE. The dotted line is in fact the locus where the product of M/L, K_V, and L_0' is constant and not simply that where M/L = constant.

Figure 4 is instead a plot of the $\log(\langle I_e\rangle)-\log(R_e)$ distribution for objects of very different masses, covering a range from $\sim 1 M_\odot$ to $\sim 10^{14} M_\odot$, i.e., from stars to clusters of galaxies. The data for the GC systems are taken from Pasquato & Bertin (2008), while those for stars are taken from the SIMBAD database.[3] The data for the galaxy clusters, ranging in mass from 10^{12} to 10^{14} solar masses, come from S. Cariddi et al. (2017, in preparation). A similar plot was done by Dantas et al. (2000) using the k-space over the range going from GCs to galaxy clusters.

Note that the $\log(\langle I_e\rangle)-\log(R_e)$ relation seems to be valid on all scales. In this figure the region of the ZOE is visible in gray. The various virialized systems are not randomly distributed. Their position in the diagram depends on their structure and luminosity. The plot demonstrates that for all kinds of virialized systems there is a similar link between structure, dynamics, and luminosity. All structures are distributed along the lines parallel to that defining the ZOE with $\beta = -2$. The position of all systems in the diagram should be determined in some way by the fine-tuning relation linking the luminosity of the stellar population and the dynamics of the system governed by the total mass.

For stars, the M^*/L ratio increases as we move farther away from the ZOE, going from the main sequence stars of A spectral type to that of M type stars. If the dominating stellar population inside a stellar system is made of late-type stars we will therefore observe a higher (M^*/L) that will likely place the galaxy far from the ZOE.[4]

Note also that this diagram is done for the V-band, so there is a natural selection effect at play, since the lower (M^*/L) (due to bright stars that dominate the galaxy luminosity) progressively moves the galaxies toward the ZOE.

[3] The selected stars span the spectral types from A0 to M5. They are: α Cor B., Sun, 70 Oph A, 61 Cyg A, EZ Aqu.

[4] Assuming that the DM contribution is approximately the same for all galaxies, which is not exactly the case.

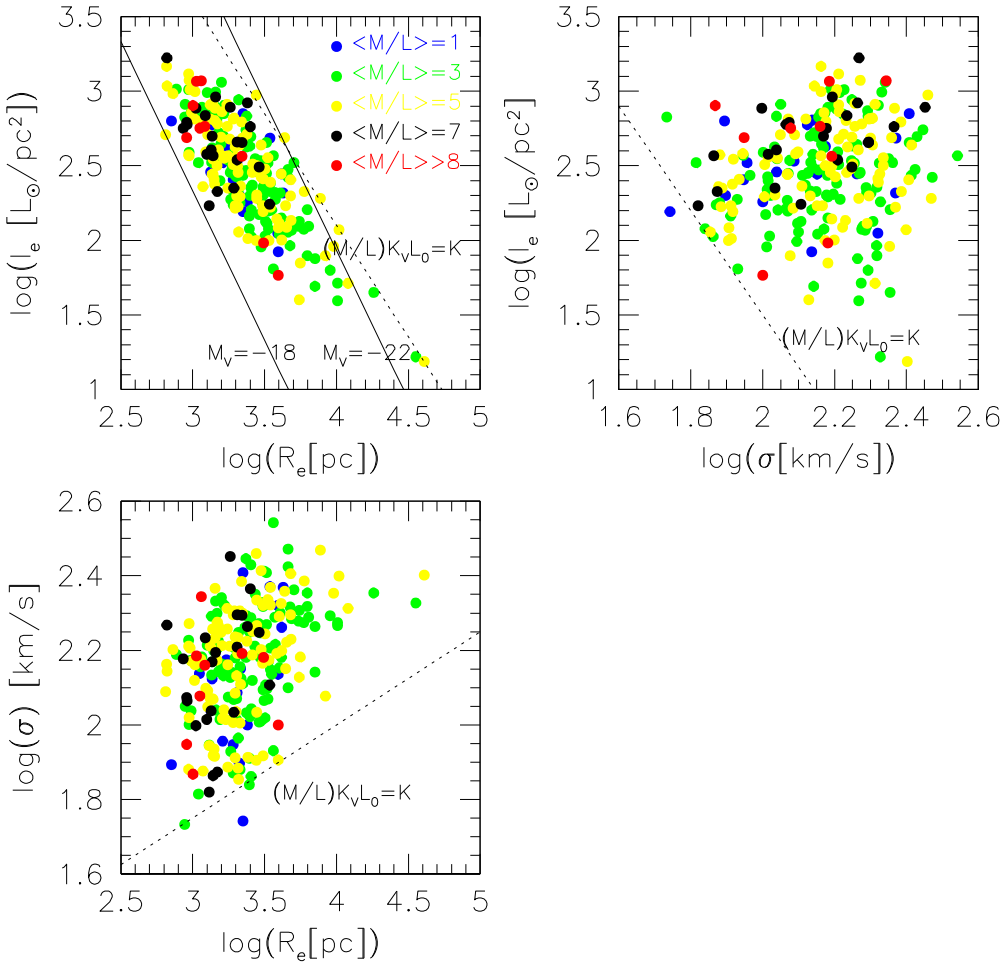

Figure 5. Different projections of the FP on the $\log(R_e)-\log(\langle I_e\rangle)-\log(\sigma)$ axes. The dotted lines mark a possible position for the ZOE. The color-coding follows Figure 3.

The galaxy clusters appear shifted with respect to the ZOE because these systems contain several spiral galaxies with low M^*/L and have a lot of DM, while globular clusters have a high mass-to-light ratio because their stellar population is dominated by stars with high (M^*/L).

For the other FP projections we obtain

$$\log(\langle I_e\rangle) = (\beta - 1)\log(\sigma) + \text{const},$$
$$\log(\sigma) = \frac{1}{2-\beta}\log(R_e) + \text{const}, \qquad (20)$$

where the constant zero-points also depend on the combination of M/L, K_V, and L_0'. Again the $\beta = -2$ value determines the distribution of galaxies and the position of the ZOE in the respective diagrams (see Figure 5).

In conclusion, the observed distribution of ETGs in the FP projections suggests that the fine-tuning between structure and stellar population could indeed be the origin of the FP properties. Each galaxy in the $\log(R_e)-\log(\langle I_e\rangle)-\log(\sigma)$ space can be represented by two virtual planes that intersect each other. The first plane is provided by the virial theorem and fixes the mass of a galaxy once the M/L and K_V are given. The other plane represents the total luminosity and comes from the $L = L_0'\sigma^{-2}$ relation, where in the parameter L_0' the role played by the SFH is encrypted.

In the next section we will further discuss the connection between luminosity, star formation, and velocity dispersion in ETGs.

5. The Connection between Luminosity, SFR, and Velocity Dispersion

We have seen that the FP could originate from a fine-tuning of the zero-points of two planes, the VP and the PFJ plane. This link implies a close connection between the SF history of ETGs and their structural and dynamical characteristics. The FP projections seem to confirm such a link in the observed nonrandom distribution of galaxies.

Here we will see that there exists a strong link between luminosity, the time-averaged SFR, and the central velocity dispersion. Equations (12) and (13) can in fact be combined as

$$L^2 = L_0\left\langle\frac{L}{M}\right\rangle\langle\Psi\rangle T_G\left(\frac{\sigma}{\sigma_0}\right)^2; \qquad (21)$$

thus it is possible to predict the validity of the following relation:

$$L = q\sqrt{\langle\Psi\rangle}\,\sigma, \qquad (22)$$

where $q = \sqrt{L_0\langle\frac{L}{M}\rangle T_G}/\sigma_0$ is a dimensional constant.

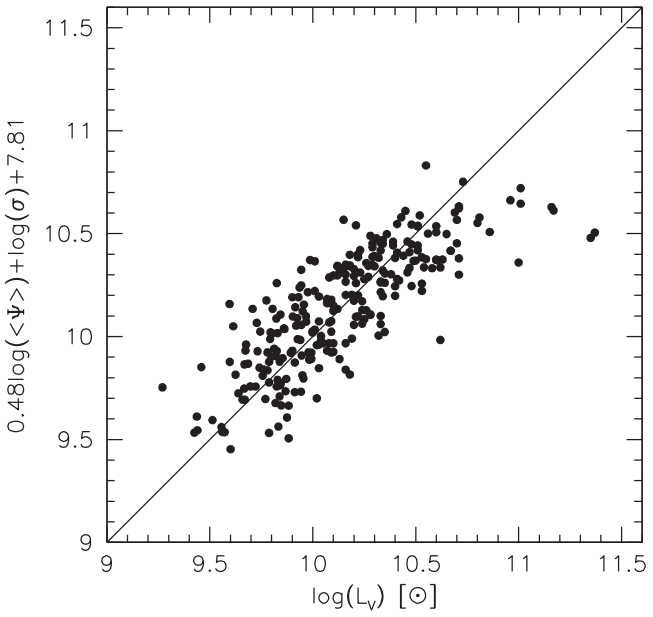

Figure 6. Mutual correlation between L, $\langle\Psi\rangle$, and σ in log units.

All these things tell us that we should look at the correlation of three variables L, σ, and $\langle\Psi\rangle$. These are mutually connected because the mass M correlates with the velocity dispersion σ through the virial relation and the light L correlates with the time-averaged SFR $\langle\Psi\rangle$. Consequently, σ and $\langle\Psi\rangle$ are connected. Figure 6 provides the observed correlation among these variables.

The 3D correlation between these variables derived with the program *R* (https://www.r-project.org) gives

$$\log(L) = 0.48(\pm0.06)\log(\langle\Psi\rangle) + 1.00(\pm0.13)\log(\sigma) + 7.81(\pm0.26), \quad (23)$$

with an rms = 0.215 (R = 0.64 and p-value $<1.2 \times 10^{-16}$). The partial correlation coefficients of $\log(L)$ with $\log(\sigma)$ and $\log(\langle\Psi\rangle)$ are respectively 0.44 and 0.43, indicating a robust 3D relation. This is in remarkable good agreement with the theoretical expectation seen above, indicating that at the basis of the zero-points variations of the VP and PFJ planes there is such connection.

6. More on the FJ and PFJ Planes

We now consider in more detail the meaning of the L–σ plane. The FJ plane contains two measured quantities, the galaxy luminosity and the stellar velocity dispersion. At variance with the VP that is defined for one galaxy only in the $\log(R_e)-\log(\langle I_e\rangle)-\log(\sigma)$ space assigning the mass and zero-point, the FJ plane contains all real galaxies at the same time. Along the fitted relation the zero-point L_0 is nearly constant for almost all galaxies (let us say between 10^9 and 10^{12} $M_\odot$).

The first thing to note is that in the FJ plane the points of constant M/L, K_V, and L_0' are the galaxies themselves (see again Figure 1). Note how the selected solution with $\beta = -2$ used for the $\log(\langle I_e\rangle)-\log(R_e)$ relation gives here the series of parallel zero-points that for each σ provide the luminosities of all galaxies reproducing the observed FJ relation when they are considered all together. The FJ relation seems to originate from the intersections of the "projections" in the L–σ space (having collapsed I_e and R_e in the variable L) of all the parallel virtual planes that represent the total luminosity of galaxies with the "projections" arising from the VPs (the dashed lines where M/L, K_V, and R_e are constants). The intersections of the $L = L_0'\sigma^{-2}$ lines with the VP projections fix the exact position of galaxies in the L–σ space. This is the relation expected for all virialized stellar systems having similar zero-points, L_0.

In this context it is therefore possible to explain why the residuals from the FJ relation correlate with the (M/L) ratio (Cappellari et al. 2006) and with galaxy sizes (Desmond & Wechsler 2016).

Figure 7 shows the FP derived here for the present ETG sample (solid line). It has been obtained following D'Onofrio et al. (2008), using the MIST fit kindly provided by F. La Barbera (2008, private communication). The FP coefficients obtained for this sample are: $a = 1.29$, $b = 0.29$ (note that here $\langle\mu\rangle_e$ has been used instead of $\langle I\rangle_e$), and $c = -7.24$.

Dwarf galaxies ($M \sim 10^{8\div9} M_\odot$), GCs, and galaxy clusters deviate from the main galaxy relation. This occurs because these systems have a zero-point in their VP and PFJ planes that systematically different, i.e., they have different M/L, K_V, and L_0' values.

The left and right panels of Figure 7 clearly show that all stellar systems behave in a similar way. All systems satisfy the FP and FJ relations, but with zero-points slightly different from that of typical galaxies. These ZP variations depend on the different links between the virialized structure and its stellar population.

The larger exponent observed in many cases for the FJ relation (4 instead of 2) in this case could ultimately depend on the heterogeneity of the galaxy sample, i.e., on the inclusion of galaxies of very different masses and luminosities. An example is seen in the right panel of Figure 7, where we get a slope of 3.26 for the FJ by fitting together all stellar systems.

In any case, the FJ law is a relation that provides a further element to the virial relation, linking mass (and the virialized system internal gravitational energy) to the production of radiant energy, i.e., to the object luminosity. The mechanisms of energy production can be very different and can yield to widely different M/L, even among stellar systems, where the mechanism is roughly the same, ultimately associated with nuclear reactions in the star interior.

If we now take Equation (18) with $\beta = -2$, giving the zero-point of the relationship between the effective surface brightness I_e and the effective radius R_e (the zero-point varies with M/L, K_V, and L_0' and hence with Z_{FP}), after a few steps we get

$$K' = \frac{K_V}{4\pi^2 G}\frac{L}{M}L_0', \quad (24)$$

where L_0' is L/σ^{-2} and K' is a parameter different for each cosmic epoch (with units of [gr^2 cm^3 s^{-6}] or [$L_\odot^2$/pc] when the normalization factor in L_0' is not taken into account), the gravitational constant is given in cgs units or expressed as $G = 4.3 \times 10^{-3}$ pc $M_\odot^{-1}$ (km/s)^2 and the term K_V is a function of the Sérsic index n (see, Bertin et al. 2002). K' will follow the evolution of the main galaxy parameters by changing the position of a galaxy in the $\log(\langle I_e\rangle)-\log(R_e)$ plane. As a consequence the whole FP is expected to vary its tilt across the cosmic epochs.

Figure 8 shows the relation between L_0' derived from Equation (24) and the total galaxy luminosity L. Here we used

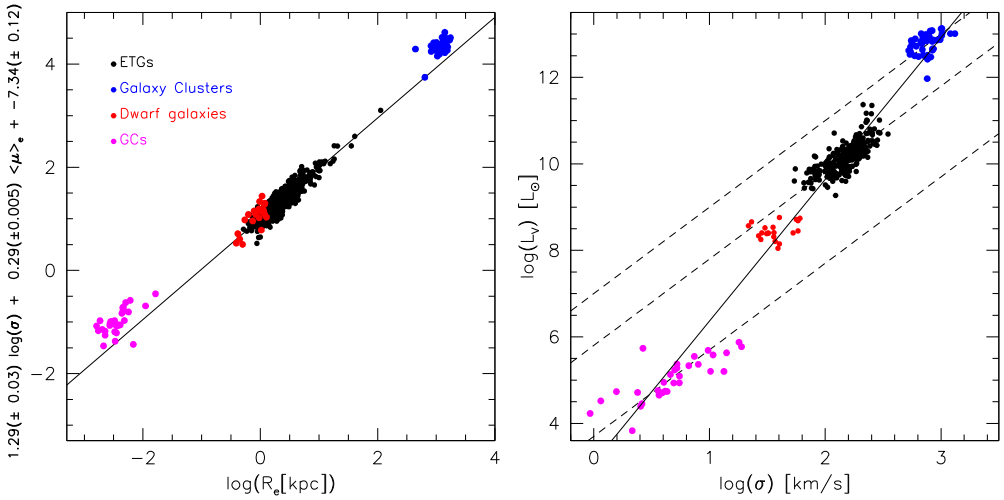

Figure 7. Left: an edge-on view of the FP for ETGs with the position of all other types of stellar systems overplotted. Right: the same systems for the FJ relation. The color-coding is the same as Figure 4. The solid line with a slope of 3.26 is obtained from fitting all systems together.

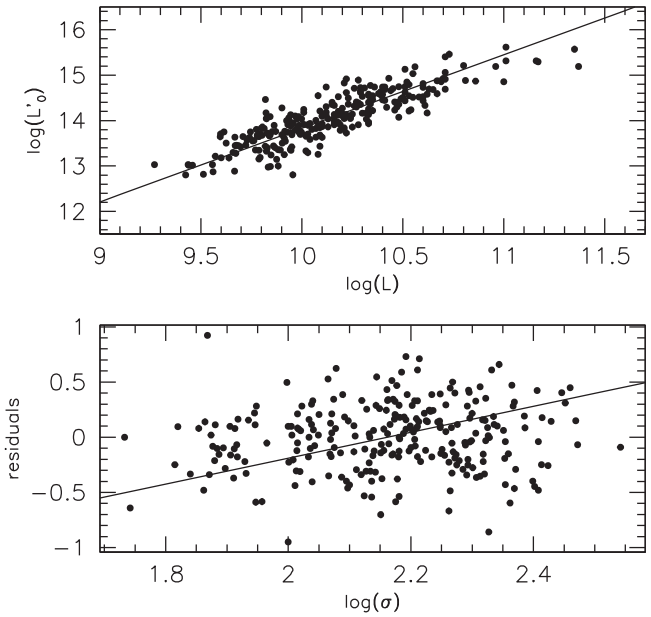

Figure 8. Upper panel: plot of L_0' derived from Equation (24) vs. the measured total galaxy luminosity L. Lower panel: plot of the residuals from the best fit of the above relation vs. the measured velocity dispersion σ in log units.

the stellar M^*/L ,with M/L being unknown for our galaxies. We observe that the link of L_0' and L is far from being trivial: L_0' is derived from a complex combination of M/L and K_V. The fit between these variables is done here with the classical unweighted bisector linear regression analysis (Feigelson & Babu 1992). We used this method because there is not an a priori dependence of one variable on the other and the errors for both are poorly determined. We note that the residuals of this relation mildly depend on the central velocity dispersion σ. The correlation coefficient is only 0.11, but the probability of a correlation by chance is $P = 6.5 \times 10^{-2}$, indicative of a possible dependence. This hidden correlation with σ provides further support to the idea that L_0' is a proxy of $\langle\Psi\rangle$ and there is a 3D dependence between luminosity, SFR, and velocity dispersion.

Furthermore, Figure 9 gives a clear indication that both L and L_0' are correlated with the time-averaged SFR of the galaxies measured by Fritz et al. (2007). The residuals of these correlations present again a significant dependence on σ. The probability of correlation by chance between the residuals of the $\log(L)-\log(\langle\Psi\rangle)$ relation and $\log(\sigma)$ is $P = 7.2 \times 10^{-1}$. For the residuals of the $\log(L_0')-\log(\langle\Psi\rangle)$ relation the probability of correlation by chance with $\log(\sigma)$ is instead $P = 2.4 \times 10^{-2}$. In both cases these correlations reveal the presence of a second hidden parameter, i.e., σ, which is significant for the 261 ETGs of our sample. This is another element in favor of the 3D relation $L-\langle\Psi\rangle-\sigma$.

In summary, we have considered two different correlations. The first one is that between mass M and velocity dispersion σ provided by the virial theorem. The second one is that between luminosity L and mean SFR $\langle\Psi\rangle$. Since mass and luminosity are connected through the M/L ratio, the FJ relation can be derived assuming that $L_0 = R_e L/GM$. The residuals of the $L-\sigma$ relation depend on $\langle\Psi\rangle$ (or proxy of it likes M^*/L), while the residuals of the $L-\langle\Psi\rangle$ relation depend on σ. It follows that the 3D relation provided by $L - \sigma - \langle\Psi\rangle$ (in log units) originates from such mutual correlations.

With this in mind we now better understand why we should use the $L = L_0'\sigma^{-2}$ relation for building the second virtual plane in the $\log(R_e)-\log(\langle I_e\rangle)-\log(\sigma)$ space. In fact, in order to build such a plane we need to use the direct correlation between L and $\langle\Psi\rangle$ that is valid for each galaxy and not the one between L and σ that is valid for all galaxies (this is in fact the VP rewritten). What we want is to express the galaxy luminosity in a way that is independent of its mass. The $L-\langle\Psi\rangle$ relation has σ as a second hidden parameter, as we have seen.

In the next section we will further explore the consequences of our findings for the problem of the star formation activity in galaxies.

7. The SF Activity in Galaxies

Equation (14) provides a link between L_0 and the mean SFR of galaxies. It does not give a direct link between the current SFR, the velocity dispersion and L_0. What we are looking for is instead a more direct link between these quantities. How are they connected? We will show in the Appendix that the FJ relation can be interpreted as a possible translation of the Stefan–Boltzmann law that is valid for stars in the case of

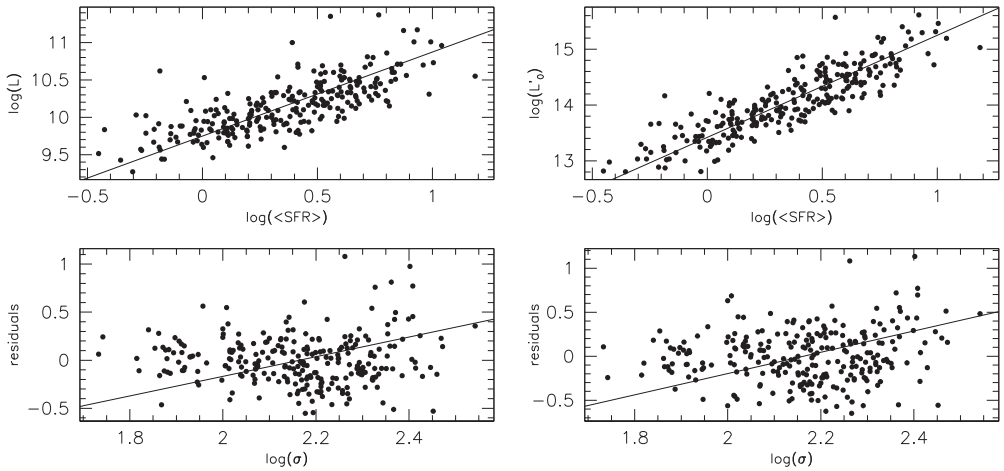

Figure 9. Left panel: plot of $\log(L)$ vs. the time-averaged SFR in log units. Right panel: plot of $\log(L_0')$ vs. the time-averaged SFR in log units. Note that the residuals of these relations depend in a mild way on $\log(\sigma)$.

stellar systems, presenting evidence that it is always possible to express the energy of a system with more convenient units (the ones we can measure).

During this exercise we noted that the galaxy luminosity can be expressed at any time t as:

$$L_G = \langle \alpha_s \rangle N_s \langle M_s v_s^2 \rangle, \tag{25}$$

where the quantities within <> are weighted time-averages over the whole stellar population. Here N_s is the number of stars in the galaxy, M_s is their mass, and v_s^2 is their velocity dispersion. The constant α_s is different for each galaxy and represents the ratio between the total energy emitted in the form of electromagnetic radiation and the total kinetic energy of a galaxy. This relation is valid for any stellar system in virial equilibrium.

In this context the quantity L_0 can be expressed by the relation

$$\frac{L_0}{\alpha_s} = M_g = \int_0^t \Psi(t) dt, \tag{26}$$

where we have explicitly written the mass of the galaxy as the integral of its star formation rate and we have highlighted the dependence on time of this parameter.

We can now recast Equations (24) and (26) differently, presenting evidence for the star formation rate of a galaxy. From this expression we can argue that at any epoch t after virialization the SFR could be given by:

$$\Psi(t) = \frac{d}{dt}\left(\frac{4\pi^2 G K'(t)}{\alpha_s(t) K_V(t)} \frac{M(t)}{L(t)} \frac{1}{\sigma^4(t)}\right). \tag{27}$$

This theoretical relation is important because it allows the derivation of the global SFR of a virialized galaxy at any time t, taking into account the structure, the dynamics, and the light produced by its stars. This relation explains why we have a fine-tuning between structure and stellar population and consequently why we observe the FP and the ZOE. The existence of the L–$\langle\Psi\rangle$–σ relation should in other words be the final output of such fine-tuning.

Equation (27) tells us that at each cosmic epoch t after virialization the SFR in a galaxy is not free. An unperturbed galaxy can form stars only at the rate permitted by Equation (27) along the whole cosmic history. In other words, once the mass and the potential well of a galaxy are given, the star formation proceeds according to the galaxy dynamics and the expected evolution of the stellar populations formed. If a galaxy does not merge with others and does not experience a significant infall of new gas, its SFR will not be modified considerably, continuing its evolution according to Equation (27). We know, however, that during their evolution ETGs experience repeated merging events and infall of gas. During big mergers galaxies are perturbed in their virial equilibrium and the validity of Equation (27) is probably lost for the time required to recover the virial equilibrium (approximately the freefall time). At the same time, large infall of gas, ram pressure events, and feedback forces could switch on/off the SFR compressing or stripping the gas component. These external influences should therefore in some way be reflected in the properties of the FP (and its projections) and the FJ relations. Variations are expected in the FP and FJ relations of ETGs when they are subject to merging and infall/quenching events perturbing the SFR. Observations of high-redshift ETGs should therefore shed light on the mechanism originating the FP.

In the case of our sample of nearby ETGs these events are exceptions. Merging and large infall or quenching events are in the far history of these objects. They had time to recover their structure (virial equilibrium) and their SFR should therefore follow the behavior expected from Equation (27). Note that for these ETGs the central velocity dispersion is high and the SFR is low. This is expected on the basis of Equation (27).

Could we test in some way the validity of Equation (27) through observations? Unfortunately, this requires a database of masses, luminosities, SFR, and velocity dispersions of galaxies at different redshifts, while our WINGS database is made up only of nearby ETGs. However, considering that at $t = 0$ the SFR was 0, we can predict that the mean SFR of today galaxies will be approximately given by:

$$\langle \Psi \rangle = \frac{L_0}{\alpha_s \Delta t} \sim \frac{1}{2} \frac{M_G}{T_G}, \tag{28}$$

where $\Delta t = T_G$ is the luminosity-weighted age of the galaxies.

Figure 10 shows the mean SFR measured by Fritz et al. (2007) in four distinct epochs from the direct fit of the galaxy SEDs versus the mean SFR obtained by Equation (28). The correlation (c.c. = 0.6 and rms $\sim$ 2.8 but significant at a $\sim 7\sigma$

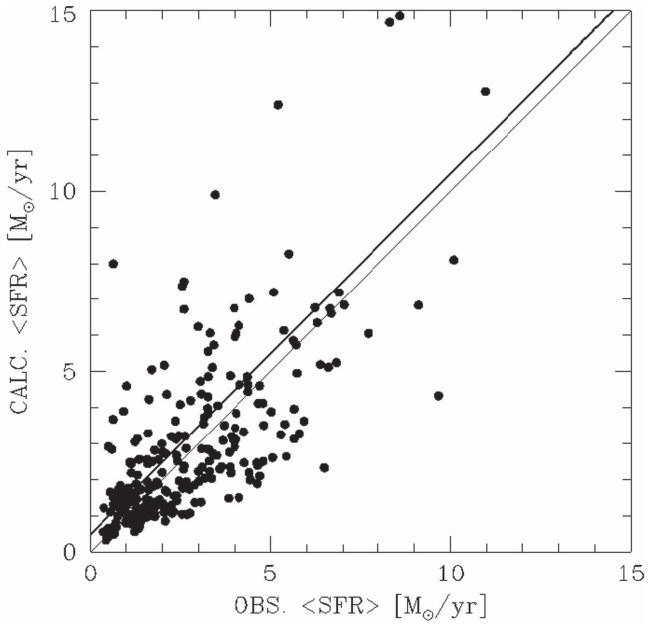

Figure 10. Plot of the mean observed SFR measured by Fritz et al. (2007) for the galaxies of the WINGS database using the fitted spectral energy distributions vs. the mean $\langle\Psi\rangle$ calculated on the basis of the prediction of Equation (27) (see the text). The thin line is the one-to-one relation, while the thick line is the fitted distribution.

confidence level) appears consistent with the theoretical expectation, taking into account the various sources of errors affecting both quantities, even if the sample is biased and the correlation may be driven by few points at high SFR values. This test gives therefore a marginal indication for the validity of Equation (27).

We believe that this equation is important to understand the FP and the SFH in galaxies. Currently, simulations are the only way to test the validity of Equation (27). To what extent could merging/feedback events change the main stream of SF that each galaxy has encrypted in it since the beginning of the virial equilibrium? At which redshift are the FP and FJ relations of ETGs in place? These are all questions for the upcoming *JWST* telescope. A study of the FP and FJ relations for high-redshift objects observed during the phases of their maximum activity in SF will likely shed more light on the validity of Equation (27).

8. Conclusions

We have shown that the origin of the FP can be traced back to the validity of two basic physical relations: the virial dynamical equilibrium and the $L-\langle\Psi\rangle-\sigma$ relation linking the galaxy luminosity, the time-averaged SFR, and the velocity dispersion. When it is written as $L = L_0'\sigma^{-2}$ this relation provides a second virtual plane in the $\log(R_e)-\log(\langle I_e\rangle)-\log(\sigma)$ space, whose zero-point varies in a coordinated way with the VP. This fine-tuning is at the origin of the properties of the FP. The coupling of these relations could also explain the existence of the downsizing phenomenon and the nature of the ZOE in the FP projections.

Since, as demonstrated by Zaritsky (2012), a fundamental manifold can be constructed for all stellar systems, the easy prediction is that in general the FP and FJ relations are different for each class of stellar system (GCs, dwarf galaxies, late-type galaxies, normal ETGs, clusters of galaxies) that are dominated by velocity dispersion. The diversity originates from the different zero-points of the VP and PFJ planes, or in other words from the different SFHs and the different coupling between structure, dynamics, and stellar populations. The combination of the virial equilibrium, the $L = L_0'\sigma^{-2}$ relation, and the validity of the PFJ law for galaxy systems constrains objects of similar characteristics to the same FP, which is the locus of constant M/L ratio, K_V, and $\langle\Psi\rangle$ at each time epoch.

The projection of the intersecting lines connecting the VP and $L = L_0'\sigma^{-2}$ planes explains the properties observed for ETGs in the $\log(\langle I_e\rangle)-\log(R_e)$ plane, in particular the existence of the ZOE that in this framework is the natural limit reached by the stellar and dynamical evolution of a stellar system today.

The existence of the FP for nearby ETGs provides a natural constraint on the possible SFR activities, and the dynamical and structural transformations that these objects might experience. Once formed and virialized in a given potential well, the global SFR of an unperturbed ETG could not deviate from the track imposed by Equation (27). In other words, the evolution of the SFR depends on the transformations in mass, luminosity, structure, and dynamics (unless new merging phenomena occur at later epochs).

Equation (27) should be studied now through photometric and dynamical simulations following the details of the mass assembly in stars and their relative luminosities. Naively, we can predict that since the stellar mass is generally increasing, while luminosity and stellar velocity dispersions could vary with the generations of stars, the resulting SFR will probably see various peaks at different redshift epochs depending on the galaxy dynamics.

It will be interesting to see if Equation (27) will help to quantify the problem of the star formation across the cosmic epochs and to constrain in some way the mass quenching phenomenon. First, it will be important to verify if the two principal types of galaxies in the color–magnitude (or stellar mass), color–concentration, and color–morphology diagrams can be reproduced (Strateva et al. 2001; Kauffmann et al. 2003; Brinchmann et al. 2004; Baldry et al. 2004, 2006; Driver et al. 2006; Bamford et al. 2009). We know that in these plots there are two main regions: the so-called blue cloud (or main sequence), where galaxy mass correlates with the star formation rate, and the red sequence where there is no such correlation and galaxies are passive. The origin of this bimodality is commonly attributed to the bulge and disk structure of galaxies. In general, disks are bluer in color than bulges (e.g., Peletier & Balcells 1996) and galaxies with lower stellar mass and lower Sérsic index tend to be bluer (and hence have higher sSFRs) than higher stellar mass and higher Sérsic index systems (Baldry et al. 2004, 2006; Driver et al. 2006; Bamford et al. 2009). Similar trends are observed for luminosity and stellar light concentration (Strateva et al. 2001; Driver et al. 2006). This idea fits with the found dependence of the SFR on the Sérsic index and the velocity dispersion found here. Unfortunately, all such relationships are complicated by the effects of the environment, so disentangling the various effects on the star formation efficiency is quite difficult.

We would like to acknowledge the anonymous referee whose comments and suggestions have greatly improved this work.

Appendix
A Possible Origin for the FJ Relation

We try to demonstrate here that the FJ relation with $\beta = 2$ could be seen as a sort of translation of the blackbody Stefan–Boltzmann law valid for individual stars for the case of a galaxy made by an assembly of stars in which the temperature is replaced by the velocity dispersion. From this analysis it will appear again that the link connecting L_0 and L_0' is the SFR of galaxies.

It goes without saying that there is not an immediate straight correlation between the physical situations in stars and galaxies; however, we will convincingly see that such an analogy is possible and also argue that dynamics (via the velocity dispersion) and stellar populations in a galaxy (via the light emitted by stars) are intimately related. To demonstrate that this is possible we proceed as follows.

A.1. The Case of Single Stars

A star of mass M_s, radius R_s, luminosity L_s, and effective temperature $T_{s,e}$ is an assembly of N heavy particles (nuclei, ions, and atoms, whereas electrons can be neglected) in thermal motion with mean temperature $\langle T \rangle$ and in virial equilibrium, i.e., satisfying the condition

$$M_s v_s^2 \equiv \left| \frac{GM_s^2}{R_s} \right| \equiv E_V, \tag{29}$$

where v_s is the mean particle velocity in a gram of matter, $M_s = N \langle m_p \rangle$, with N as the number of heavy particles and m_p as their mean mass, and finally E_V stands for the "virial energy."

Consider first the total bolometric luminosity of a star (i.e., the total energy emitted per second by the surface). This is usually derived from the Stefan–Boltzmann law, since stars are in good approximation blackbody systems.

In a star we can measure the luminosity L_s, the effective temperature $T_{\rm es}$, and the radius R_s, which are related by the well known blackbody law ($L = 4\pi R^2 \sigma_{\rm SB} T^4$), where $\sigma_{\rm SB}$ is the Stefan–Boltzmann constant. The suffix SB is to distinguish it from the velocity dispersion of stars in a galaxy, usually indicated with the same symbol. When misunderstanding is obviously avoided, the suffix is dropped.

It is worth recalling here that the luminosity can be derived from the energy content of the blackbody according to

$$U_{\rm bb}(T) = \frac{8\pi\Omega}{h^3c^3}(kT)^4 \frac{\pi^4}{15}, \tag{30}$$

where Ω is the total volume and $U_{\rm bb}(T)$ is the total energy of the blackbody. From this we obtain the luminosity of the star

$$L_s = \frac{U_{\rm bb}(T)}{\Omega} 4\pi R_s^2 c = \frac{3U_{\rm bb}(T)c}{R_s}. \tag{31}$$

At this point we verify that the gravitational energy, the mean kinetic energy of the particles, and the blackbody energy content of the whole star with mean temperature $\langle T \rangle$ are comparable to each other. Taking the Sun as a typical star, for which we assume $R_s = 6.94\ 10^{10}$ cm, $M_s = 1.99\ 10^{33}$ g, mean internal temperature $\langle T \rangle \simeq 5 \times 10^6$ K, and central value[5] $T \simeq 10^7$, we obtain:

(i) the mean density of kinetic energy of the N particles in the star is

$$\langle E_k \rangle = \frac{1}{\Omega} \sum_i^N \frac{m_p v_p^2}{2} = \frac{3}{2} nKT \simeq 3.47 \times 10^{15}\ {\rm erg\ cm^{-3}}, \tag{32}$$

where m_p and v_p are the mass and velocity of each particle and $n = N/\Omega$ is the number density of particles;

(ii) the mean density of gravitational energy is

$$\langle E_g \rangle = \frac{3GM_s^2}{4\pi R_s^4} \simeq 2.72 \times 10^{15}\ {\rm erg\ cm^{-3}}; \tag{33}$$

(iii) the mean energy density of the photons is

$$\langle U_{\rm bb}(T) \rangle = \frac{8\pi^5}{15h^3c^3}(KT)^4 \simeq 1.15 \times 10^{15}\ {\rm erg\ cm^{-3}}; \tag{34}$$

for a mean temperature of 10^7 K. Within the numerical approximation the three energies are of the same order. Strictly speaking, one should have $\langle E_g \rangle \simeq \langle E_k \rangle + \langle U_{\rm bb} \rangle$. Within the approximation, our estimates fulfill this constraint. Analogous estimates can be made for other types of stars with similar conclusions. In other words, there seems to be a relationship between the gravitational energy density and the sum of the electromagnetic and kinetic energy densities. Finally, using the virial condition we can also estimate the mean velocities of the particles in a star (the Sun in this example), which are about $v_s \simeq 200\ {\rm km\ s^{-1}}$, depending on the exact value adopted for the temperature.

Given these premises, the luminosity of a star can be derived from

$$L_s = \left| \frac{dE_i}{dt} \right|, \tag{35}$$

where E_i is the total internal energy (sum of the nuclear and gravothermal contributions). We may generalize the above relation by supposing that the luminosity can be expressed as

$$L_s = \alpha_s E_V \equiv \alpha_s M_s \langle v_p \rangle^2 \equiv \alpha_s \langle U_{\rm bb} \rangle \frac{4}{3}\pi R_s^3, \tag{36}$$

where α_s is a suitable proportionality factor with the dimension of an inverse of time. In other words, we link the luminosity L_s to the internal properties of the star, in particular to the mean velocity of the constituent heavy particles.

However, the same luminosity can be expressed by means of the surface blackbody with a temperature equal to the effective

[5] The elementary theory of stellar evolution by combining the equations for hydrostatic equilibrium, mass conservation, and physical state of the plasma, e.g., $P = \frac{k}{\mu m_H}\rho T$, provides a simple relation for the mean temperature inside a star

$$\bar{T} \geqslant 4.58 \times 10^6 \mu \frac{M}{M_\odot}\frac{R_\odot}{R}\ {\rm K},$$

where M and R are the total mass and radius of the star and μ is the mean molecular weight of the gas. For a solar-like star $\mu \simeq 1$, so $\bar{T} \simeq 5 \times 10^6$. The central temperature is higher than this and close to 10^7.

temperature T_e of the star (a few thousand degrees, about 5.78×10^3 K for the Sun and 3×10^3 for a RGB star).

$$L = \langle U'_{\rm bb} \rangle 4\pi c R_s^2, \quad (37)$$

where $U'_{\rm bb}$ is the energy of the blackbody at the surface temperature. This implies that the ratio of the external to the internal blackbody energies is $U'_{\rm bb} \simeq 10^{-13} U_{\rm bb}$. The size of the proportionality coefficient can be understood as being due to the T^4 dependence of the blackbody energy density and the natural variation of the temperature from the surface to the inner regions of a star. The typical temperature gradient of a Sun-like star is $\|\Delta T/\Delta R\| \simeq 10^{-4}$ K cm^{-1}, where $\Delta T = T - T' \simeq T$ and $\|\Delta R\| = \|R - R'\| \simeq R'$ if R and T refer to an inner region (close to the center) and R' and T' to the surface. Therefore,[6] $T'/T \simeq 10^{-4}$.

It follows from all this that $\alpha_s \simeq 10^{-14} c/R_s$. Inserting the value for the light velocity and the radius of a typical star (like the Sun) one obtains $\alpha_s \simeq 10^{-14}$ s^{-1}.

The factor c/R_s ensures that the energy density is translated to energy lost per unit time (a power). What we have done so far is a simple rephrasing of the classical expression for the luminosity. The reason for writing the star luminosity in this curious way will become clear as soon as we move to galaxies, i.e., to systems hosting billions of stars.

The whole discussion above has been checked against stars like the Sun, so it follows that changing the types of stars should also change the value of α_s. This is shown in Figure 11. As expected α_s spans a wide range passing from dwarfs to massive stars, but this will not affect our final conclusions.

A.2. The Case of Galaxies

We now extend the above consideration and formalism to the case of a galaxy with mass M_G and radius R_G, a large assembly of stars, each of them shining with the luminosity $L_{s,i}$. In brief, the luminosity of the galaxy is the sum of the luminosity of all the stars inside; the luminosity of each star can be expressed as being proportional to the total kinetic energy of gas particles. Therefore we may write

$$L_G = \sum_{i=1}^{N_s} \alpha_{s,i} M_{s,i} v_{s,i}^2, \quad (38)$$

where N_s is the total number of stars within the galaxy, and $\alpha_{s,i}$, $M_{s,i}$, $v_{s,i}$, and $R_{s,i}$ are the basic quantities characterizing each star. In analogy with Equation (36), the galaxy luminosity can be rewritten as

$$L_G = \langle \alpha_s \rangle N_s \langle M_s v_s^2 \rangle, \quad (39)$$

where the quantities within <> are weighted averages over the whole stellar population. Note that for galaxies of the same "size" (mass and radius) these values will be very similar.

Now, thanks to the homologous nature of the gravitational collapse at all scales, it is possible to note that the quantity $\langle v_s \rangle$, i.e., the mean velocity of particles inside a star, turns out to be comparable to the velocity dispersion of stars within a galaxy, customarily named σ (in km s^{-1}). It is then possible to write

$$L = L_0 \sigma^2, \quad (40)$$

where

$$L_0 = \langle \alpha_s \rangle N_s \langle M_s \rangle \equiv \langle \alpha_s \rangle M_G. \quad (41)$$

It can be shown that even for a galaxy there is a relationship between the total gravitational energy, the total kinetic energy of the stars, and the total radiative energy emitted by stars that allows the relation (41) to be replaced by

$$L_0 = \langle \alpha_G \rangle M_G \equiv \frac{c}{R_G} M_G, \quad (42)$$

where α_G refers to the galaxy as a whole. Like in the case of stars, $\langle \alpha_G \rangle$ has the dimension of an inverse of time.

To demonstrate the validity of Equation (42) we consider a generic mean stellar content of $N_s \simeq 10^{12}$ objects, for simplicity taken to be like the Sun ($M_\odot = 2 \times 10^{33}$ g and radius $R_\odot = 6.94 \times 10^{10}$ cm, surface temperature $T_s \simeq 5780$ K), total mass $M_G = 10^{12} M_\odot$, total radius $R_G \simeq 100$ kpc. In this example we ignore the contribution to the mass given by DM. According to the current understanding of the presence of DM in galaxies, the ratios of the dark to baryonic matter (BM) both in mass and radii of the spatial distributions (supposed to be spherical) are $M_{\rm DM} \simeq \beta \times M_{\rm BM}$ and $R_{\rm DM} = \beta \times R_{\rm BM}$. This means that within the volume occupied by the BM there is about $1/\beta^2 \times M_{\rm DM}$ (Bertin et al. 1992; Saglia et al. 1992; Bertin et al. 2002). For current estimates of $\beta \simeq 6$ DM can be neglected in the internal regions of a galaxy where stars are located.

The energy density of the photons emitted by all the stars in the galaxy evaluated at any arbitrary point inside the galaxy is

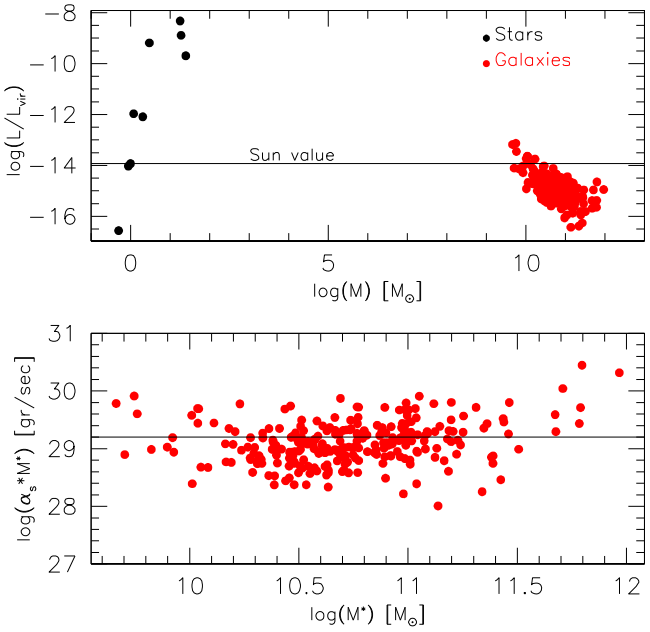

Figure 11. Upper panel: plot of α_s for the stars and its analog for the galaxies α_G (see the text for the definition) as a function of the mass of the virialized system (star or galaxy as appropriate). Note the large range of values spanned by α_s by varying the mass of the star from a dwarf to a massive object. Finally, note that the values α_G for the galaxies fall in a range typical of the low-mass (old) stars. Lower panel: plot of $L_0 = \alpha_s * M_G$ (using M^* instead of M_G) vs. the galaxy masses. The solid line gives the value observed for L_0 in the FJ relation.

[6] The values assumed for the central and surface temperature of the Sun amply justify a ratio $T'/T \simeq 0.0001$ or lower and a proportionality factor 10^{-13} in the relationship between the energy densities $U_{\rm bb}$ and $U'_{\rm bb}$.

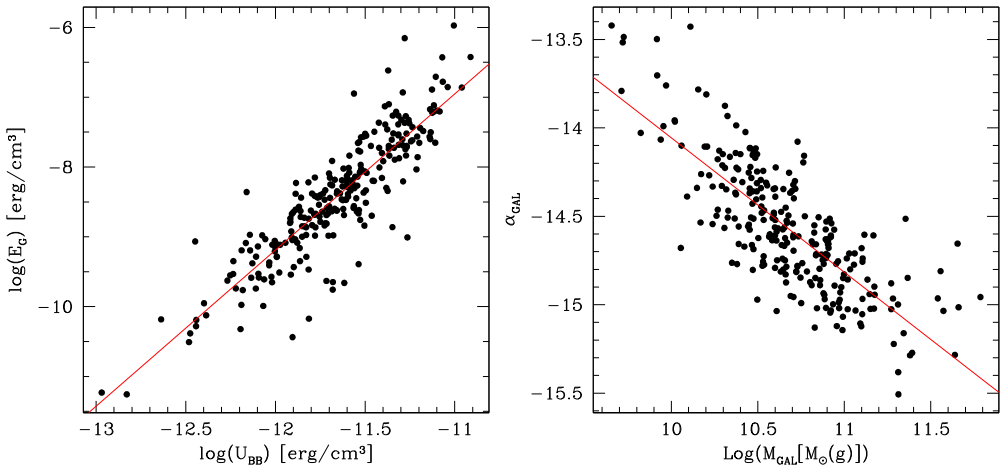

Figure 12. Left panel: the mean density of the gravitational energy vs. the mean density of the BB energy for a sample of early-type galaxies. Right panel: the quantity α_G as a function of the stellar galaxy mass in solar units for an object from the same sample.

given by

$$U_{\mathrm{bb},G} = \int_0^{R_G} U'_{\mathrm{bb},s} \frac{N_s}{\Omega_G} \quad 4\pi r^2 dr \frac{R_s^2}{r^2}, \tag{43}$$

where $U'_{\mathrm{bb},s}$ refers to the blackbody at the temperature of the stellar sources[7], Ω_G is the volume of the whole galaxy, and the factor $U'_{\mathrm{bb},s} \times N_s/\Omega_G$ is the mean blackbody radiation inside the galaxy. Although the integrand of Equation (43) is not strictly correct for evaluating the variation of the blackbody energy as a function of the galactocentric distance, it is adequate for our purposes. The quantity $U'_{\mathrm{bb},s}$ is given by

$$U'_{\mathrm{bb},s} = \frac{8\pi}{h^3c^3}\frac{\pi^4}{15}(kT)^4 \simeq 8.02 \text{ erg cm}^{-3}, \tag{44}$$

so for $U_{\mathrm{bb},G}$ of Equation (43) we estimate

$$U_{\mathrm{bb},G} \simeq 1.29 \times 10^{-12} \text{ erg cm}^{-3}, \tag{45}$$

where we assumed $N_s \simeq 10^{12}$ stars, $R_s \simeq 6.94 \times 10^{10}$ cm (roughly the solar radius), $\Omega_G \simeq 1.13 \times 10^{71}$ cm^3 for a galactic radius of about 100 kpc.

The mean density of kinetic energy of the stars turns out to be of the order of 3.52×10^{-12} erg cm^{-3} for a mean velocity dispersion of about 200 km s^{-1}.

The mean gravitational energy density for the galaxy (limited to the volume occupied by the BM) is

$$E_{g,G} = G\frac{M_G^2}{R_G^4}\frac{3}{4\pi} \simeq 7.79 \times 10^{-12} \text{ erg cm}^{-3}. \tag{46}$$

The gravitational energy is surely underestimated because we have neglected the presence of DM.

Therefore, also in this case there is an approximate relationship between the gravitational energy and the sum of electromagnetic and kinetic energy densities.

We can then write the equation

$$L_G = \alpha_G M_G \sigma^2 = \alpha_G \langle U_G \rangle R_G^3. \tag{47}$$

Thanks to the assumption of a uniform distribution of stars and stellar types contributing to the light in our model galaxy, the distribution of the photon energy inside is also uniform and always equal to that of many blackbodies of similar temperature. Furthermore, owing to the very large number of stars in a galaxy, the light emitted by a certain region, e.g., within the effective radius, can be assimilated into that of a blackbody at a certain mean temperature and very large surface. Therefore we may write

$$L_G = \langle U_{\mathrm{bb},G} \rangle 4\pi c R_G^2, \tag{48}$$

so for solar-like stars $\alpha_G \simeq c/R_G \simeq 10^{-13}$ s$^{-1} \simeq \alpha_s$. It is worth emphasizing here that α_G is nearly identical to α_s and for each galaxy there is a star with similar α.

In conclusion, the classical FJ relationship $L = L_0\sigma^2$ can be understood as a sort of translation of the Stefan–Boltzmann law for blackbodies (BBs) to the case of galaxies that can be viewed as the sum of many BBs.

Figure 11 shows the range of values for the parameter α_G of galaxies and compares them with those for stars. Note that low-mass galaxies have in general higher values of α (closer to the values for intermediate-mass stars), whereas the larger galaxies are preferentially populated by low-mass stars. What matters here is that for every galaxy there exists a combination of L_0 ($\sim\alpha_s M_G$) and σ able to reproduce the total galaxy luminosity. The lower panel of Figure 11 shows that $L_0 = \alpha_s * M_G$ is approximately constant for a wide range of galaxy masses.

We have calculated $U_{\mathrm{bb},G}$ and E_g for a small sample of nearby early-type galaxies (Moretti et al. 2014) for which all the basic data were available, and we have estimated the parameter α_G for all of them. The results are shown in the two panels of Figure 12.

One can debate whether this is also true for spiral galaxies. We believe that the origin of the Tully–Fisher relation (Tully & Fisher 1977) for late-type systems can likely be reported to the same context. Here the mean characteristic velocity of the stellar system is no longer the velocity dispersion, but the circular rotation. For more complex systems, where rotation and velocity dispersion are significant, a combination of the

[7] In relation to this, we remind the reader that in most nearby galaxies the detected light is due to stars from the main sequence turnoff (or slightly fainter than) to the tip of the RGB. In sufficiently old galaxies the corresponding mass range is rather small. In other words, the stellar population responsible for the observed light can be reduced to a single population of a certain age and mean chemical composition.

two is required to characterize the total kinetic energy. That issue, however, is left to a future investigation.

References

Baldry, I. K., Balogh, M. L., Bower, R. G., et al. 2006, MNRAS, 373, 469
Baldry, I. K., Glazebrook, K., Brinkmann, J., et al. 2004, ApJ, 600, 681
Bamford, S. P., Nichol, R. C., Baldry, I. K., et al. 2009, MNRAS, 393, 1324
Bender, R., Burstein, D., & Faber, S. M. 1992, ApJ, 399, 462
Bernardi, M., Sheth, R. K., Annis, J., et al. 2003, ApJ, 125, 1866
Bertin, G., Ciotti, L., & Del Principe, M. 2002, MNRAS, 386, 149
Bertin, G., Saglia, R. P., & Stiavelli, M. 1992, ApJ, 384, 423
Bolton, A. S., Treu, T, Koopmans, L. V. E., et al. 2008, ApJ, 684, 248
Borriello, A., Salucci, P., & Danese, L. 2001, MNRAS, 341, 1109
Brinchmann, J., Charlot, S., White, S. D. M., et al. 2004, MNRAS, 351, 1151
Burkert, A. 1993, A&A, 278, 23
Burstein, D., Bender, R., Faber, S. M., & Nolthenius, R. 1997, AJ, 114, 1365
Busarello, G., Capaccioli, M., Longo, G., & Puddu, E. 1997, in ASP Conf. Ser. 166, The Second Stromlo Symp. "The Nature of Elliptical Galaxies," ed. M. Arnaboldi, G. S. Da Costa, & P. Saha (San Francisco, CA: ASP), 184
Caon, N., Capaccioli, M., & D'Onofrio, M. 1993, MNRAS, 265, 1013
Capaccioli, M. 1987, in Structure and Dynamics of Elliptical Galaxies, ed. P. T. de Zeeuw (Dordrecht: Reidel), 47
Capaccioli, M. 1989, in The World of Galaxies, ed. H. G. Corwin & L. Bottinelli (Berlin: Springer), 208
Capaccioli, M., Caon, N., & D'Onofrio, M. 1992, MNRAS, 259, 323
Capelato, H. V., de Carvalho, R. R., & Carlberg, R. G. 1995, ApJ, 451, 525
Cappellari, M., Bacon, R., Bureau, M., et al. 2006, MNRAS, 366, 1126
Cappellari, M., McDermid, R. M., Alatalo, K., et al. 2012, MNRAS, 432, 1862
Cava, A., Bettoni, D., Poggianti, B., et al. 2009, A&A, 495, 707
Cenarro, A. J., Cardiel, N., Gorgas, J., et al. 2001, MNRAS, 326, 959
Chiosi, C., Bressan, A., Portinari, L., & Tantalo, R. 1998, A&A, 339, 355
Ciotti, L., Lanzoni, B., & Renzini, A. 1996, MNRAS, 282, 1
Dantas, C. C., Ribeiro, A. L. B., Capelato, H. V., & de Carvalho, R. R. 2000, ApJL, 528, L5
de Carvalho, R. R., & da Costa, L. N. 1988, ApJS, 68, 173
Dekel, A., & Cox, T. J. 2006, MNRAS, 370, 1445
Desmond, H., & Wechsler, R. H. 2016, arXiv:160404670D
Djorgovski, S., & Davis, M. 1987, ApJ, 313, 59
Djorgovski, S., De Carvalho, R., & Han, S. M. 1988, ASPC, 4, 329
D'Onofrio, M., Bindoni, D., Fasano, G., et al. 2014, A&A, 572, 87
D'Onofrio, M., Fasano, G., Moretti, A., et al. 2013, MNRAS, 435, 45
D'Onofrio, M., Fasano, G., Varela, J., et al. 2008, ApJ, 685, 875
Dressler, A., Lynden-Bell, D., Burstein, D., et al. 1987, ApJ, 313, 42
Driver, S. P., Allen, P. D., Graham, A. W., et al. 2006, MNRAS, 368, 414
Faber, S. M., Dressler, A., Davies, R., Burstein, D., & Lynden-Bell, D. 1987, in Nearly Normal Galaxies: From the Planck time to the Present; Proc. Eighth Santa Cruz Summer Workshop in Astronomy and Astrophysics 1987 (New York: Springer), 175
Faber, S. M., & Jackson, R. E. 1976, ApJ, 204, 668
Fasano, G., Marmo, C., Varela, J., et al. 2006, A&A, 445, 805
Fasano, G., Vanzella, E., Dressler, A., et al. 2012, MNRAS, 420, 926
Feigelson, E. D., & Babu, G. J. 1992, ApJ, 397, 55
Forbes, D. A., Ponman, T. J., & Brown, R. J. N. 1998, ApJL, 508, L43
Fritz, J., Poggianti, B. M., Bettoni, D., et al. 2007, A&A, 470, 137
Gargiulo, A. 2009, MNRAS, 397, 75
Gerhard, O., Kronawitter, A., Saglia, R. P., & Bender, R. 2001, AJ, 121, 1936
Graham, A., & Colless, M. 1997, MNRAS, 287, 221
Graves, G. J., Faber, S. M., & Schiavon, R. P. 2009, ApJ, 698, 1590
Hjorth, J., & Madsen, J. 1995, ApJ, 445, 55
Hopkins, P. F., Cox, T. J., & Hernquist, L. 2008, ApJ, 689, 17
Hyde, J. B., & Bernardi, M. 2009, MNRAS, 396, 1171
Kauffmann, G., Heckman, T. M., Tremonti, C., et al. 2003, MNRAS, 346, 1055
Kormendy, J. 1977, ApJ, 218, 333
La Barbera, F., de Carvalho, R. R., de La Rosa, I. G., & Lopes, P. A. A. 2010, MNRAS, 408, 1335
La Barbera, F., Ferreras, I., Vazdekis, A., et al. 2013, MNRAS, 433, 3017
La Barbera, F., Pasquali, A., Ferreras, I., et al. 2014, MNRAS, 445, 1977
Magoulas, C., Springob, C. M., Colless, M., et al. 2012, MNRAS, 427, 245
Michard, R. 1985, A&AS, 59, 205
Moretti, A., Poggianti, B. M., Fasano, G., et al. 2014, A&A, 564, 138
Nigoche-Netro, A., Aguerri, J. A. L., Lagos, P., et al. 2010, A&A, 516, A96
Nipoti, C., Londrillo, P, & Ciotti, L. 2006, MNRAS, 370, 681
Omizzolo, A., Fasano, G., Reverte Paya, D., et al. 2009, A&A, 561, 111
Oñorbe, J., Domínguez-Tenreiro, R., Sáiz, A., Serna, A., & Artal, H. 2005, ApJL, 632, L57
Pahre, M. A., De Carvalho, R. R., & Djorgovski, S. G. 1998, AJ, 116, 1606
Pasquato, M., & Bertin, G. 2008, A&A, 489, 1079
Peletier, R. F., & Balcells, M. 1996, AJ, 111, 2238
Prugniel, P., & Simien, F. 1997, A&A, 321, 111
Refregier, A. 2003, ARA&A, 41, 645
Renzini, A., & Ciotti, L. 1993, ApJL, 416, L49
Robertson, B., Cox, T. J., Hernquist, L., et al. 2006, ApJ, 641, 21
Saglia, R. P., Bertin, G., & Stiavelli, M. 1992, ApJ, 384, 433
Schombert, J. M. 1986, ApJS, 60, 603
Scodeggio, M., Gavazzi, G., Belsole, E., Pierini, D., & Boselli, A. 1998, MNRAS, 301, 1001
Secco, L. 2001, NewA, 6, 339
Secco, L., & Bindoni, D. 2009, NewA, 14, 567
Sheth, R. K., & Bernardi, M. 2012, MNRAS, 422, 1825
Smith, R. J., Hudson, M. J., Nelan, J. E., et al. 2004, AJ, 128, 1558
Strateva, I., Ivezić, Ž., Knapp, G. R., et al. 2001, AJ, 122, 1861
Terlevich, A. I., & Forbes, D. A. 2002, MNRAS, 330, 547
Tortora, C., Napolitano, N. R., Romanowsky, A. J., Capaccioli, M., & Covone, G. 2009, MNRAS, 396, 1132
Treu, T., Ellis, R. K., Liao, T. X., & van Dokkum, P. G. 2005, ApJL, 622, L5
Trujillo, I., Burkert, A., & Bell, E. F. 2004, ApJ, 127, 1917
Tully, B. R., & Fisher, J. R. 1977, A&A, 54, 661
Valentinuzzi, T., Woods, D., Fasano, G., et al. 2009, A&A, 501, 851
van Dokkum, G., & Conroy, C. 2010, Natur, 468, 940
Varela, J., D'Onofrio, M., Marmo, C., et al. 2009, A&A, 497, 667
Vikhlinin, A., Kravtsov, A., Forman, W., et al. 2006, ApJ, 640, 691
Young, C. K., & Currie, M. J. 1994, MNRAS, 268, 11
Zaritsky, D. 2012, ISRAA, 2012, 189625